Journal of
Applied Crystallography

ISSN 0021-8898

Received 24 December 2007
Accepted 28 July 2008

Quantitative estimation of incompatibility stresses and elastic energy stored in ferritic steel

A. Baczmanski,[a]* P. Lipinski,[b] A. Tidu,[c] K. Wierzbanowski[a] and B. Pathiraj[d]

[a]Faculty of Physics and Applied Computer Science, AGH-University of Science and Technology, al. Mickiewicza 30, 30-059 Kraków, Poland, [b]LFM, Ecole Nationale d'Ingénieurs de Metz, ENIM, Ile du Saulcy, F57045 METZ Cedex 1, France, [c]LETAM, UMR CNRS 7078, Ecole Nationale d'Ingénieurs de Metz, Ile du Saulcy, F57045 METZ Cedex 1, France, and [d]Laboratory of Mechanical Automation, Faculty of Engineering Technology, University of Twente, PO Box 217, 7500 AE Enschede, The Netherlands. Correspondence e-mail: baczman@ftj.agh.edu.pl

Plastic incompatibility second-order stresses were determined for different orientations of a polycrystalline grain, using X-ray diffraction data and results of the self-consistent elasto-plastic model. The stresses in cold rolled ferritic steel were determined both in as-received and under tensile loaded conditions. It has been shown that the Reuss model and the self-consistent model applied to near surface volume provide the best approaches to determine diffraction elastic constants. For the first time, the elastic energy in an anisotropic material (arising from plastic incompatibilities between grains having various lattice orientations) has been determined. The second-order incompatibility stresses and stored elastic energy are presented in Euler space.

1. Introduction

The diffraction method is a powerful tool for determining the stress field in polycrystalline materials. The stresses acting in polycrystalline grains cause an elastic deformation of the crystal lattice, which will result in shifts in diffraction peak positions as compared with those from the same material in the stress-free condition. The measurement of peak shifts for different orientations of the scattering vector with respect to the sample enables the stress determination. The stresses present in the near surface volume are usually determined using the well known $\sin^2\psi$ method (Noyan & Cohen, 1987). If only the macrostresses (the first-order stresses) are present in a quasi-isotropic material (with random orientations of the grains lattice), the measured interplanar spacing $\langle d(\varphi, \psi)\rangle_{\{hkl\}}$ will be a linear or elliptical function of $\sin^2\psi$ [φ and ψ are defined in Fig. 1(*a*)]. In such a case, the macrostress tensor can be determined from measured $\langle d(\varphi, \psi)\rangle_{\{hkl\}}$ *versus* $\sin^2\psi$ curves (Noyan & Cohen, 1987; Welzel *et al.*, 2005).

In the case of a textured material, the $\langle d(\varphi, \psi)\rangle_{\{hkl\}}$ *versus* $\sin^2\psi$ curves are neither linear nor elliptical. These deviations (called nonlinearities) of the measured $\sin^2\psi$ plots are due to the elastic anisotropy of the material. Such nonlinearities can be well predicted by various methods that are used to determine the diffraction elastic constants (Welzel *et al.*, 2005). The calculations are based on the crystallographic texture and single-crystal elastic constants, and they predict the character of $\sin^2\psi$ plots for a sample under applied (or residual) macrostresses. However, in the case of plastically deformed polycrystalline material, the interpretation of nonlinearities of $\sin^2\psi$ plots based on the elastic anisotropy alone is insufficient.

Another reason for the nonlinearities of the measured $\sin^2\psi$ plots is the effect of plastic incompatibility stresses (second-order stresses), which develop during elasto-plastic deformations of the sample (Greenough, 1949; Marion & Cohen, 1977; Hauk, 1986; Pintschovius *et al.*, 1987). A number of authors have attempted to explain the nonlinear character of $\sin^2\psi$ plots as being due to the incompatibilities of polycrystalline grains arising from the differences in their plastic flow properties; these differences are caused by variations in the lattice orientations of the grains with respect to the applied load (Greenough, 1949; Shiraiwa & Sakamoto, 1970; Taira *et al.*, 1971). Later, the Taylor model and the self-consistent model of elasto-plastic deformation were used to predict the nonlinearities of the $\sin^2\psi$ plots (Van Acker *et al.*, 1994; Krier, 1993). The experimental data were successfully compared with theoretical results; however, the plastic incompatibility stresses were not determined.

Independently of theoretical calculations, diffraction experiments with multiple reflections were performed to determine plastic incompatibility stresses directly from the lattice strains measured on a group of crystallites (Willemse *et al.*, 1982; Hauk, 1986; Hauk *et al.*, 1988; Pintschovius *et al.*, 1987). However, this direct method of microstress analysis can be applied only if the crystallographic texture is significant and if it can be decomposed to a number of well defined preferred orientations. In this case, the plastic incompatibility stresses can be determined for the major texture components.

Significant effort has been made to determine the so-called stress orientation function from the lattice strains measured for many orientations of the scattering vector using different *hkl* reflections. The stress components dependent on lattice

orientations were expanded into generalized spherical harmonics (Bunge, 1982; Wang *et al.*, 1999, 2003; Behnken, 2000) and correlated with the measured lattice strains. To describe the dependence of the stress tensor on lattice orientation, functions for six independent components have to be found, contrary to the case of orientation distribution function analysis, where only a scalar function is needed (Bunge, 1982). Consequently, the solution is possible only if at least five or six independent *hkl* reflections are used to measure the strains for different orientations of the scattering vector (usually such measurements are not possible owing to the low intensity of the measured diffraction peaks, especially for textured materials). Even when sufficient experimental data are available, the solution is not unique and additional assumptions, such as the minimum of the stress or strain variance (Behnken, 2000, 2002) or a stress–strain relation based on Hill's constraint tensor (Wang *et al.*, 2001, 2003), are needed. However, it has not been proved that the obtained solution will be unique when the additional assumptions are introduced.

Concurrently, a methodology of determining stresses based on the analysis of the physical behaviour of crystallites in a polycrystalline material was proposed and developed by Baczmański and co-workers (Baczmański *et al.*, 1994, 1997, 2004; Baczmański, Braham & Seiler, 2003). This method allows quantitative evaluation of the macrostresses and the plastic incompatibility stresses using diffraction data and the self-consistent model. By analyzing the nonlinear $\langle d(\varphi, \psi)\rangle_{\{hkl\}}$ *versus* $\sin^2\psi$ curves measured using one *hkl* reflection, the plastic incompatibility stresses in cold rolled ferritic steel (Baczmański *et al.*, 1994, 1997) and in duplex steel (Inal *et al.*, 1999) were estimated. A more general multi-reflection method for determination of stresses in anisotropic materials has been elaborated by Baczmański, Braham & Seiler (2003) and Wroński *et al.* (2007). In the present work, the method of determining the macrostresses and plastic incompatibility stresses is applied to plastically deformed ferritic steel samples under an applied load.

2. Theoretical principles

2.1. Physical origins of stresses in a grain

Stresses are generated in elastic materials when subjected to an external load or a thermo-mechanical treatment changing the relative shapes or volumes of different parts of the body. Usually the stress field is heterogeneous and anisotropic. In numerous processes the changes in the internal structure after the treatment are permanent and lead to development of residual stresses. To fully describe the residual stress field in a polycrystalline material, the stresses in a single grain, as well as in a macroscopic volume V containing a large number of grains, must be considered (for example, the volume contributing to diffraction).

Owing to the large-scale heterogeneity of the irreversible plastic deformation, non-zero residual loads are created at the boundaries of the given volume V of the sample. The mean stresses related to these loads are called the $\sigma^{\rm M}_{mn}$ macrostresses. The grain elastic constants, defined with respect to the sample, vary with orientation (**g**) of the crystal lattice and they may differ significantly between the grains belonging to different phases. Consequently, different values of so-called elastic grain stresses $\sigma^{g(\rm er)}_{ij}(\mathbf{g})$ will result from *elastic responses* of grains within the considered volume V to the loads applied. From linear elasticity, the elastic grain stress $\sigma^{g(\rm er)}_{ij}(\mathbf{g})$ can be related to the macrostress, *i.e.*

$$\sigma^{g(\rm er)}_{ij}(\mathbf{g}) = B^{g}_{ijmn}(\mathbf{g})\,\sigma^{\rm M}_{mn}, \qquad (1)$$

where $\mathbf{B}^{g}(\mathbf{g})$ is the stress concentration tensor and summation over repeated indices is applied.

It should be noted that the elastically induced stresses $\sigma^{g(\rm er)}_{ij}(\mathbf{g})$ linearly depend on the macrostress values and they disappear when $\sigma^{\rm M}_{mn} \rightarrow 0$ [equation (1)]. The stress concentration tensor can be calculated for each grain (within volume V) using different models (Mura, 1993; Lipinski & Berveiller, 1989; Clyne & Withers, 1993). It will depend on the elastic anisotropy of the individual grains and of the whole sample (crystallographic texture), elastic coupling between the grains, and the presence of different phases.

During deformation of a polycrystalline material, the irreversible incompatibilities caused by varying plastic flow in different grains will lead to *plastic incompatibility* stresses $\sigma^{g(\rm ic)}_{ij}(\mathbf{g})$. These stresses will remain in the grains even when the

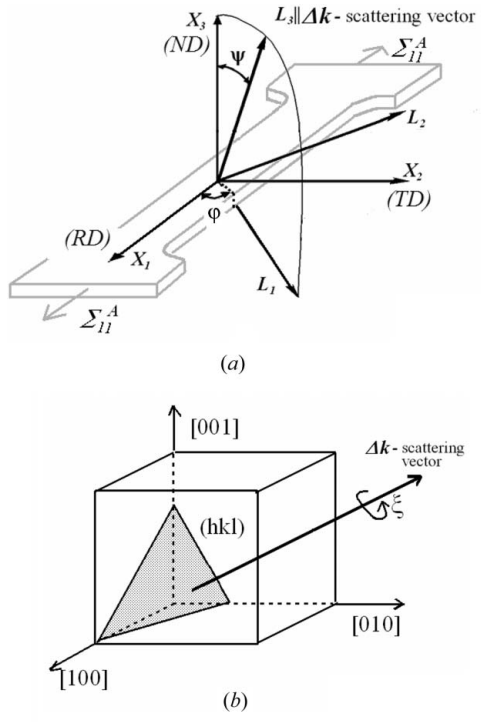

Figure 1
(*a*) Orientation of the laboratory system **L** with respect to the sample system **X** given by the ψ and φ angles; the L_3 axis is parallel to the scattering vector $\Delta\mathbf{k}$, and the uniaxial stress $\Sigma^{\rm A}_{11}$ is applied along the X_1-axis direction. Directions of rolling: the RD (rolling), TD (transverse) and ND (normal) directions are indicated. (*b*) Definition of lattice rotation around the scattering vector $\Delta\mathbf{k}$ normal to the (*hkl*) plane.

external force is removed, *i.e.* when $\sigma_{mn}^{\rm M} \rightarrow 0$. The grain stress $\sigma_{ij}^{g}(\mathbf{g})$ can be expressed as a superposition of a term $\sigma_{ij}^{g(\rm er)}(\mathbf{g})$ [dependent on the macrostresses defined by equation (1)] and another term $\sigma_{ij}^{g(\rm ic)}(\mathbf{g})$ describing the plastic incompatibility of a particular grain, *i.e.*

$$\sigma_{ij}^{g}(\mathbf{g}) = \sigma_{ij}^{g(\rm er)}(\mathbf{g}) + \sigma_{ij}^{g(\rm ic)}(\mathbf{g}). \quad (2)$$

Using equation (1), the stress in the grain can be related to the macrostresses acting in the volume V, *i.e.*

$$\sigma_{ij}^{g}(\mathbf{g}) = B_{ijmn}^{g}(\mathbf{g})\,\sigma_{mn}^{\rm M} + \sigma_{ij}^{g(\rm ic)}(\mathbf{g}). \quad (3)$$

2.2. Diffraction method for stress determination

In the present work, the modified $\sin^2\psi$ diffraction method (Baczmański *et al.*, 1994; Baczmański, Braham & Seiler, 2003) is applied to determine stresses in a cold rolled ferritic steel sample. This method is based on the measurements of interplanar spacing for various orientations of the scattering vector, defined by the φ and ψ angles (see Fig. 1*a*). According to equation (3), the grain stress and the lattice strain depend on the macrostresses $\sigma_{ij}^{\rm M}$ and the plastic incompatibility stresses $\sigma_{mn}^{g(\rm ic)}(\mathbf{g})$. Consequently, in the case of a single-phase material the measured mean lattice strain, $\langle\varepsilon(\varphi,\psi)\rangle_{\{hkl\}}$, will be composed of two terms,[1] *i.e.*

$$\langle\varepsilon(\varphi,\psi)\rangle_{\{hkl\}} = F_{ij}(hkl,\varphi,\psi)\,\sigma_{ij}^{\rm M} + \langle\gamma_{3m}\,\gamma_{3n}\,s_{mnij}^{g}(\mathbf{g})\,\sigma_{ij}^{g(\rm ic)}(\mathbf{g})\rangle_{\{hkl\}}, \quad (4)$$

where $\langle\varepsilon(\varphi,\psi)\rangle_{\{hkl\}}$ is the mean lattice elastic strain in the $\mathbf{L}_3$ direction for crystallites having the scattering vector perpendicular to the $\{hkl\}$ planes, $F_{ij}(hkl,\varphi,\psi)$ are the diffraction elastic constants (described below), $s_{mnij}^{g}(\mathbf{g})$ are the single-crystal elastic constants defined with respect to the $\mathbf{X}$ system, $\mathbf{g}$ denotes grain orientation and γ_{km} are elements of the matrix transforming strains and stresses from the sample ($\mathbf{X}$) to the laboratory ($\mathbf{L}$) coordinate system (see Fig. 1*a*).

According to the methodology proposed by Baczmański *et al.* (1994) the anisotropy of the incompatibility stresses can be predicted qualitatively by the self-consistent model. However, the absolute values of the stresses will depend on the hardening and relaxation processes occurring during plastic deformation. These processes are difficult to model and in general the amplitude of the stress tensors is not correctly predicted. To relate the magnitude of theoretical stresses to the actual ones, an unknown scaling factor q is introduced in the modified $\sin^2\psi$ method (Baczmański *et al.*, 1994, 2004; Baczmański, Braham & Seiler, 2003). This factor does not depend on the grain orientation $\mathbf{g}$ and it rescales the amplitude of the stress tensor, *i.e.* the incompatibility stress $\sigma_{ij}^{g(\rm ic)}(\mathbf{g})$ in the real sample is equal to

$$\sigma_{ij}^{g(\rm ic)}(\mathbf{g}) = q\,\overline{\sigma_{ij}^{g(\rm ic)}(\mathbf{g})}, \quad (5)$$

where q is the scaling parameter and $\overline{\sigma_{ij}^{g(\rm ic)}(\mathbf{g})}$ is the plastic incompatibility stress for a grain with orientation $\mathbf{g}$ as predicted by the model.

Finally, by defining the measured lattice strain as

$$\langle\varepsilon(\varphi,\psi)\rangle_{\{hkl\}} = \frac{\langle d(\varphi,\psi)\rangle_{\{hkl\}} - d_{\{hkl\}}^{0}}{d_{\{hkl\}}^{0}}, \quad (6)$$

the experimental interplanar spacings $\langle d(\varphi,\psi)\rangle_{\{hkl\}}$ obtained from the diffraction method can be expressed as

$$\langle d(\varphi,\psi)\rangle_{\{hkl\}} = \Big[F_{ij}(hkl,\varphi,\psi)\,\sigma_{ij}^{\rm M} + q\,\overline{\langle\gamma_{3m}\,\gamma_{3n}\,s_{mnij}^{g}(\mathbf{g})\,\sigma_{ij}^{g(\rm ic)}(\mathbf{g})\rangle_{\{hkl\}}}\Big]d_{\{hkl\}}^{0} + d_{\{hkl\}}^{0}, \quad (7)$$

where $\overline{\langle\gamma_{3m}\,\gamma_{3n}\,s_{mnij}^{g}(\mathbf{g})\,\sigma_{ij}^{g(\rm ic)}(\mathbf{g})\rangle_{\{hkl\}}}$ are the model-predicted strains caused by the plastic incompatibility stresses, $\langle d(\varphi,\psi)\rangle_{\{hkl\}}$ is the mean interplanar spacing for the $\{hkl\}$ planes in the direction of the scattering vector and $d_{\{hkl\}}^{0}$ is the strain-free interplanar spacing.

Using the least-squares method for equation (7), the fitting parameters (*i.e.* $\sigma_{ij}^{\rm M}$, q and $d_{\{hkl\}}^{0}$) can be determined. The procedure used in this work is based on minimizing the merit function, denoted χ^2, which is defined as

$$\chi^2 = \frac{1}{N-M}\sum_{n=1}^{N}\left[\frac{\langle d(\varphi_n,\psi_n\rangle_{\{211\}}^{\rm exp} - \langle d(\varphi_n,\psi_n\rangle_{\{211\}}^{\rm cal}}{\delta_n}\right]^2, \quad (8)$$

where $\langle d(\varphi_n,\psi_n\rangle_{\{211\}}^{\rm exp}$ and $\langle d(\varphi_n,\psi_n\rangle_{\{211\}}^{\rm cal}$ are the experimental and calculated interplanar spacings [equation (7)], $\delta_n = \delta_n[\langle d(\varphi,\psi)\rangle_{\{hkl\}}]$ is the measurement error (standard deviation) of the determined spacing $\langle d(\varphi,\psi)\rangle_{\{hkl\}}$ for the nth measurement, and N and M are the number of measured points and fitting parameters, respectively.

We emphasize that the term $q\,\overline{\langle\gamma_{3m}\,\gamma_{3n}\,s_{mnij}^{g}(\mathbf{g})\,\sigma_{ij}^{g(\rm ic)}(\mathbf{g})\rangle_{\{hkl\}}}$ in equation (7), characterizing the nonlinearities of the $\sin^2\psi$ plot, is adjusted to the experimental data by varying the q parameter. Thus, only the amplitude of the theoretical function $\overline{\langle\gamma_{3m}\,\gamma_{3n}\,s_{mnij}^{g}(\mathbf{g})\,\sigma_{ij}^{g(\rm ic)}(\mathbf{g})\rangle_{\{hkl\}}}$ is rescaled by the q factor, while its dependence on the orientation of the scattering vector (*i.e.* on φ and ψ) is given by the model. When the value of q is determined by a fitting procedure, the real values of the plastic incompatibility stresses $\sigma_{ij}^{g(\rm ic)}(\mathbf{g})$ can be calculated for all grain orientations $\mathbf{g}$ using equation (5). Thus, the macrostresses $\sigma_{ij}^{\rm M}$ and the plastic incompatibility stresses $\sigma_{ij}^{g(\rm ic)}(\mathbf{g})$ can be estimated.

To illustrate the level of the plastic incompatibility stresses in a statistical grain, the average equivalent residual stress $[\sigma_{\rm eq}^{g(\rm ic)}]$ is calculated:

$$\big[\sigma_{\rm eq}^{g(\rm ic)}\big] = \frac{1}{8\pi^2}\int_{\mathbf{E}}\sigma_{\rm eq}^{g(\rm ic)}(\mathbf{g})\,f(\mathbf{g})\,{\rm d}\mathbf{g}, \quad (9)$$

where

[1] A more general formula for two-phase material was derived by Wroński *et al.* (2007), where the incompatibility stresses $\sigma_{ij}^{g(\rm ic)}(\mathbf{g})$ were defined as the superposition of the average phase incompatibility stresses $\sigma_{ij}^{\rm ph(ic)}$ and second-order incompatibility stresses for this phase. However, in single-phase material $\sigma_{ij}^{\rm ph(ic)} = 0$, and consequently the grain incompatibility stresses are equal to the second-order incompatibility stresses [as defined by Wroński *et al.* (2007)], *i.e.* $\sigma_{ij}^{g(\rm ic)}(\mathbf{g}) = \sigma_{ij}^{\rm II(ic)}(\mathbf{g})$.

$$\sigma_{\rm eq}^{g({\rm ic})} = \big\{(1/2)\big[(\sigma_{11}^{g({\rm ic})} - \sigma_{22}^{g({\rm ic})})^2 + (\sigma_{11}^{g({\rm ic})} - \sigma_{33}^{g({\rm ic})})^2 + (\sigma_{22}^{g({\rm ic})} - \sigma_{33}^{g({\rm ic})})^2\big] + 3\big[(\sigma_{12}^{g({\rm ic})})^2 + (\sigma_{13}^{g({\rm ic})})^2 + (\sigma_{23}^{g({\rm ic})})^2\big]\big\}^{1/2}$$

is the equivalent stress calculated according to the von Mises formula for a grain with orientation **g**, and the integral is calculated over the whole orientation space **E** using the $f(\mathbf{g})$ orientation distribution function (Bunge, 1982) as the weighting parameter.

In the next sections, the contributions of the macrostresses and incompatibility stresses to the lattice strains [equation (4)] are described.

2.2.1. Contribution of macrostresses to lattice strains. If the incompatibility stresses are not present in the material, the relation between lattice strains $\langle\varepsilon(\varphi,\psi)\rangle_{\{hkl\}}$ measured using the *hkl* reflection and macrostresses can be expressed by the linear equations (Dölle, 1979; Brakman, 1987; Barral *et al.*, 1987; Welzel *et al.*, 2005)

$$\begin{aligned}\langle\varepsilon(\varphi,\psi)\rangle_{\{hkl\}} &= F_{ij}(hkl,\varphi,\psi)\sigma_{ij}^{\rm M} \quad \text{or}\\ \langle\varepsilon(\varphi,\psi)\rangle_{\{hkl\}} &= R_{ij}(hkl,\varphi,\psi)\sigma_{ij}'^{\rm M},\end{aligned} \tag{10}$$

where $\sigma_{ij}'^{\rm M}$ and $\sigma_{ij}^{\rm M}$ are the macrostresses expressed in the **L** and **X** systems (Fig. 1*a*), respectively; $R_{ij}(hkl,\varphi,\psi)$ and $F_{ij}(hkl,\varphi,\psi)$ denote the corresponding diffraction elastic constants defined for the *hkl* reflection and the orientation of the scattering system given by the angles φ and ψ.

The relation between these two types of diffraction elastic constants is given by the equation

$$F_{ij}(hkl,\varphi,\psi) = \gamma_{mi}\,\gamma_{nj}\,R_{mn}(hkl,\varphi,\psi). \tag{11}$$

Different approaches have been proposed to calculate the $R_{ij}(hkl,\varphi,\psi)$ diffraction elastic constants for quasi-isotropic and textured materials [for example, the geometrical mean approach (Baczmański *et al.*, 1993; Matthies & Humbert, 1995)]. The classical methods are based on the assumptions of homogenous stress in the Reuss (1929) model or homogenous strain in the Voigt (1928) model, while in the self-consistent model, the elastic interaction of ellipsoidal inclusion with the homogenous matrix is considered (Kröner, 1961; Kneer, 1965; Lipinski & Berveiller, 1989). The methods for calculation of diffraction elastic constants are widely described in the literature (Dölle, 1979; Brakman, 1987; Baczmański *et al.*, 1993; Hauk, 1997; Welzel *et al.*, 2005).

Recently a new approach based on the directional dependence of grain interaction has been proposed, to calculate the diffraction elastic constants of thin coatings in which the grains are built as a two-dimensional aggregate having different in-plane and normal properties (Van Leeuwen *et al.*, 1999; Welzel *et al.*, 2003; Welzel & Fréour, 2007). It is assumed that, for crystallites with a columnar structure (having dimensions equal to the thickness of the film), the grains exhibit the same in-plane strain (a Voigt-type behaviour), whereas they can deform freely in the direction perpendicular to the coating surface (a Reuss-type behaviour). To determine the diffraction elastic constants, a grain-interaction approach based on the Vook–Witt method (Witt & Vook, 1968) was developed and applied for a general stress state in a textured material (Van Leeuwen *et al.*, 1999; Welzel *et al.*, 2003; Welzel & Fréour, 2007).

In the present work, the classical methods [*i.e.* the Reuss and Voigt methods as defined by Brakman (1987), Baczmański *et al.* (1993) and Welzel *et al.* (2005)] and the methods based on the self-consistent elastic model were applied to calculate the diffraction elastic constants for anisotropic samples [the experimental $f(\mathbf{g})$ orientation distribution function was used in the calculations]. Considering the interaction of the grain with a surrounding matrix as given by equation (1) and by using the self-consistent model approach, the diffraction elastic constants R_{mn} can be expressed as (Baczmański, Skrzypek *et al.*, 2003; Baczmański, Braham & Seiler, 2003)

$$R_{mn} = \frac{\sum\limits_{\{hkl\}}\left[\int\limits_{2\pi}^{0} s_{33ij}'^{g}(\mathbf{g})\,B_{ijmn}'^{g}(\mathbf{g})\,f(\mathbf{g})\,{\rm d}\xi\right]_{hkl}}{\sum\limits_{\{hkl\}}\left[\int\limits_{2\pi}^{0} f(\mathbf{g})\,{\rm d}\xi\right]_{hkl}}, \tag{12}$$

where $B_{ijmn}'^{g}(\mathbf{g})$ are the components of the stress concentration tensor calculated by the model and $s_{klij}'^{g}(\mathbf{g})$ are the single-crystal compliances (the prime denotes that the quantity is defined in the **L** coordinate system). The integral is calculated over the volume of all grains having orientations corresponding to crystallites rotated by $\xi(\mathbf{g})$ – the angle around the $\mathbf{\Delta k}$ scattering vector (Fig. 1*b*) – while the summation is performed for all symmetrically equivalent planes $\{hkl\}$.

Two different models are used to calculate the $\mathbf{B}'^{g}(\mathbf{g})$ tensor from equation (1). The first, which is a standard method, is based on the self-consistent model applied to an ellipsoidal inclusion embedded in a homogenous matrix (Lipinski & Berveiller, 1989; Baczmański, Skrzypek *et al.*, 2003; Baczmański, Braham & Seiler, 2003), *i.e.*

$$B_{ijmn}'^{g}(\mathbf{g}) = B_{ijmn}'^{g({\rm sc})}(\mathbf{g}). \tag{13}$$

This approach represents interaction of grains inside the sample volume and is termed the 'self-consistent interior method'.

In the second model, called the 'surface-free self-consistent method', the directional dependence of grain interaction (as in the Vook–Witt method) is incorporated into the self-consistent calculations (see also Baczmański *et al.*, 2006). In this case, the influence of a free surface is considered, assuming that grains on the surface can be freely deformed in the normal direction. Owing to absorption of X-rays, surface grains contribute more to diffraction than the grains that lie deeper in the sample. Consequently, the following scheme for grains in the near surface volume (Fig. 2) is proposed: the forces and stresses normal to the surface act similarly as in the Reuss model (free deformation in the normal direction), while a two-dimensional elastic coupling between the grains occurs in the plane parallel to the sample surface (which is calculated by the self-consistent model). Taking an approach similar to that in equation (1), the grain stresses $\sigma_{ij}^{g({\rm er})}$ can be related to the macrostresses by the concentration tensor $\mathbf{B}^{{\rm g(sc-fs)}}$, *i.e.*

$$\sigma_{ij}^{g(\mathrm{er})}(\mathbf{g}) = B_{ijmn}^{g(\mathrm{sc-fs})}(\mathbf{g})\,\sigma_{mn}^{\mathrm{M}}. \quad (14)$$

The tensor must be calculated for an inclusion on the surface of the sample. All quantities are expressed in the **X** coordinate system (see Fig. 1*a*).

The main difficulty is to calculate the tensor $\mathbf{B}^{g(\mathrm{sc-fs})}(\mathbf{g})$, which is different from that defined for an inclusion completely embedded in the material. To emulate the conditions of flat grains with a free surface, a special construction of the stress concentration tensor expressed in the **X** system is proposed, *i.e.*

$$B_{ijmn}^{g}(\mathbf{g}) = B_{ijmn}^{g(\mathrm{sc-fs})}(\mathbf{g}) = \begin{cases} I_{ijmn} & \text{for } i=3 \text{ or } j=3 \Rightarrow \text{as in Reuss model} \\ B_{ijmn}^{g(\mathrm{sc})}(\mathbf{g}) & \text{for } i\neq 3 \text{ and } j\neq 3 \Rightarrow \text{as in self-consistent bulk model,} \end{cases} \quad (15)$$

where **I** is the identity tensor and $\mathbf{B}^{g(\mathrm{sc})}$ is the concentration tensor calculated for an inclusion completely embedded in the material. The calculated $\mathbf{B}^{g}(\mathbf{g})$ tensor is then transformed to the **L** system and used in equation (12) as $\mathbf{B}'^{g}(\mathbf{g})$.

The free-surface method presented above was tested by Baczmański *et al.* (2006), by comparing theoretical and measured diffraction elastic constants for cold rolled ferritic steel. It was shown that, by using this new approach, the diffraction elastic constants of a textured sample can be calculated accurately.

2.2.2. Contribution of plastic incompatibility stresses – calculation model. To determine the contribution of incompatibility stresses on the measured lattice strain, the theoretical values of the $\sigma_{ij}^{g(\mathrm{ic})}(\mathbf{g})$ stresses must be computed using the self-consistent model. In the model, the evolution of grain properties occurring as a result of slip on crystallographic planes and elastic deformation under applied local stress is considered. The slip is active on a slip system $[uvw](hkl)$ (denoting the slip direction and plane, respectively) when the resolved shear stress exceeds the critical value $\tau_{[uvw](hkl)} = \tau_{\mathrm{c}}$. The multiplication of dislocations and their spatial distribution inside a grain will lead to a hardening due to the interaction of different slip systems, *i.e.* τ_{c} increases with deformation. The rate of increase of the critical shear stress on the *s*th system can be approximated using the work hardening matrix **H**,

$$\dot{\tau}_{\mathrm{c}}^{s} = \sum_{t} H^{st}\dot{\gamma}^{t}, \quad (16)$$

where $\dot{\gamma}^{t}$ is the rate of plastic slip on the *t*th active system and the dot denotes the time derivative. In this work, the hardening is assumed to be isotropic and linear, *i.e.* all components of the **H** matrix have the same value *H*, which does not depend on the grain deformation or other evolution parameters.

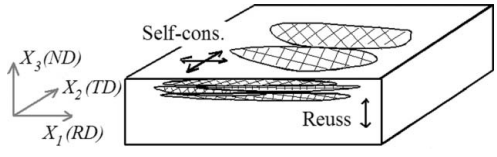

Figure 2
Scheme of interaction between elongated and flat grains in the near-surface volume for a cold rolled sample, *i.e.* Reuss model in the X_3-axis direction and the self-consistent model in the plane X_1X_2.

Table 1
Chemical composition of ULC96 ferritic steel (in wt%).

C	Si	Mn	Cr	Al	Fe
0.002	0.012	0.195	0.016	0.058	Balance

It was found in our previous work (Baczmański *et al.*, 1994) that the orientation distribution function calculated by the self-consistent model quantitatively differs from the experimental one, when the model calculations are performed for large plastic deformations (of about 50–90%) on initially randomly orientated grains. To avoid such a disagreement, a new approach is applied in the present work. The self-consistent calculations (Lipinski & Berveiller, 1989; Zattarin *et al.*, 2000) are performed for a set of grains having initially zero stresses and the distribution of lattice orientations (**g**) corresponding to the experimentally determined crystallographic texture. To simulate the cold rolling process, the following form of the strain tensor is applied to the sample during calculations:

$$\mathbf{E}^{\mathrm{rol}} = \begin{bmatrix} E_{11}^{\mathrm{rol}} & 0 & 0 \\ 0 & 0 & 0 \\ 0 & 0 & -E_{11}^{\mathrm{rol}} \end{bmatrix}. \quad (17)$$

The elasto-plastic deformation is modelled for a few percent of elasto-plastic deformation, up to a certain value of the total sample macrostrain E_{11}^{rol}. Finally, after unloading of the stresses applied to the sample, denoted by $\Sigma_{ij}^{\mathrm{rol}}$ (*i.e.* when $\Sigma_{ij}^{\mathrm{rol}} \rightarrow 0$), the theoretical stress tensor $\overline{\sigma_{ij}^{g(\mathrm{ic})}(\mathbf{g})}$ for each grain and the lattice strains

$$\overline{\langle \varepsilon_{33}^{\prime g(\mathrm{el})}(\varphi,\psi)\rangle_{\{hkl\}}} = \overline{\langle \gamma_{3m}\,\gamma_{3n}\,s_{mnij}^{g}(\mathbf{g})\,\sigma_{ij}^{g(\mathrm{ic})}(\mathbf{g})\rangle_{\{hkl\}}}$$

are calculated. In the next step, the fitting procedure based on equation (7) is applied to compute the χ^2 parameter. Such a procedure is repeated for a few different values of macrostrain (E_{11}^{rol}) to find the best agreement of the theoretically predicted anisotropy of the incompatibility stresses with the experimental data. In subsequent calculations, the model results for which the χ^2 parameter reaches a minimum value are used.

3. Analyses of experimental data using the self-consistent model

3.1. Experimental technique

Two samples were prepared from an ultra low carbon ferritic steel (ULC96) which had been cold rolled to a reduction of 96% in thickness. The chemical composition of this steel is given in Table 1. By electrochemical polishing, layers of 200 and 100 µm material were removed in the ULC96_1 and ULC96_2 samples, respectively. This was necessary to remove any surface artefacts or irregularities.

The $\langle d(\varphi,\psi)\rangle_{\{211\}}$ *versus* $\sin^2\psi$ curves were measured using an improved Rigaku X-ray Stress Analyser (MSF-2M)

equipped with a parallel beam optics and filtered Cr $K\alpha$ X-ray radiation ($\lambda_{K\alpha}$ = 0.2291 nm). The measurements were carried out using the side-inclination method (ψ-goniometer geometry). In each measurement, diffraction profiles for the 211 reflection were obtained in 13–17 different ψ directions [φ is fixed; see Fig. 1(*a*)]. The measured X-ray intensity profiles were corrected for background, Lorenz polarization, absorption (LPA) and $K\alpha_1/K\alpha_2$ overlap. A least-squares fit was applied to the resulting $K\alpha_1$ diffraction profile to calculate the peak position ($2\theta_{peak}$), from which the $\langle d(\varphi, \psi)\rangle_{\{211\}}$ values at different ψ tilt angles were determined using Bragg's law. X-ray measurements at different φ angles were performed after rotating the goniometer by an angle φ with respect to the sample axis. To perform the measurements on the sample under a uniaxial load, a mechanical tensile test machine was used. In this test machine, a constant load was maintained during the X-ray measurements. The X-ray measurements were performed at different applied load levels characterized by tensile stresses denoted by Σ_{11}^{ten}. The samples were instrumented with strain gauges on both sides to account for any bending and were calibrated beforehand. The applied tensile forces were also measured using a load cell. Using this experimental setup, it was possible to perform X-ray measurements at different φ, ψ and applied stress levels.

The nonlinearities of the measured interplanar spacing $\langle d(\varphi, \psi)\rangle_{\{211\}}$ for different orientations of the scattering vector confirmed a strong anisotropy of the plastic incompatibility stresses in the plastically deformed (cold rolled) steel (Fig. 3*a*). To illustrate that the nonlinearities of the $\langle d(\varphi, \psi)\rangle_{\{211\}}$ *versus* $\sin^2\psi$ curves are caused by incompatibility stresses, one of the cold rolled samples was subsequently annealed. After annealing, the nonlinearity significantly decreased as expected, since the plastic incompatibility residual stresses were reduced (Fig. 3*b*).

3.2. Diffraction elastic constants and theoretical incompatibility stresses

The experimental orientation distribution function, presented in Fig. 4(*a*), and the single-crystal elastic constants given in Table 2 were used to calculate different types of diffraction elastic constants.

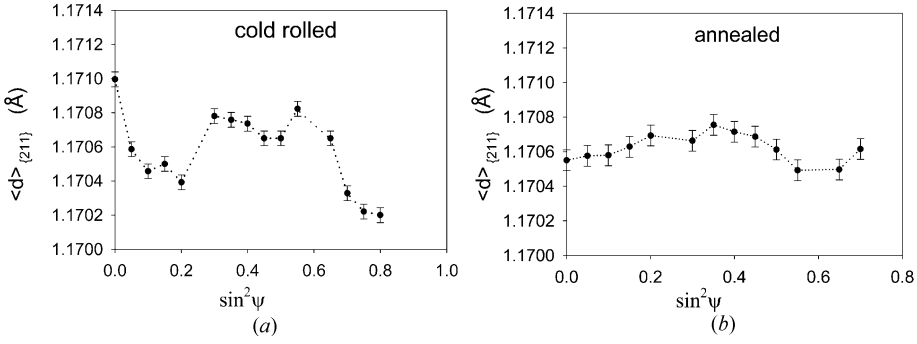

Figure 3
Exemplary $\langle d(\varphi, \psi)\rangle_{\{211\}}$ *versus* $\sin^2\psi$ curves measured for cold rolled (*a*) and annealed (*b*) steel samples.

Table 2
Parameters used in the prediction model.

τ_c is the critical resolved shear stress and H is the hardening parameter.

	Single crystal elastic constants (GPa)				
Assumed slip systems	c1111	c1122	c1212	τ_c (MPa)	H (MPa)
⟨111⟩{211} and ⟨111⟩{110}	231	134	116	250	80

To determine the theoretical stresses $\overline{\sigma_{ij}^{g(ic)}}(\mathbf{g})$, the deformation due to the cold rolling process was simulated using the self-consistent model [the sample strain tensor $\mathbf{E}^{rol}$ is defined in equation (17)]. The polycrystalline sample was represented by 10 000 grains having (initially) zero values of the stress components and a distribution of lattice orientations (**g**) corresponding to the experimentally determined texture (Fig. 4*a*). The calculations were performed up to different values of the sample strains E_{11}^{rol} [see equation (17)], using the parameters given in Table 2. The fitting procedure based on equation (7) was applied to adjust the theoretical $\langle d(\varphi, \psi)\rangle_{\{211\}}$ *versus* $\sin^2\psi$ functions to the experimental results for the as-received ULC96_1 sample. The values of the χ^2 parameter were determined using $\overline{\sigma_{ij}^{g(ic)}}(\mathbf{g})$ stresses obtained for different macrostrains E_{11}^{rol}. The diffraction elastic constants calculated by the self-consistent method for a free surface were used and an uncertainty of 0.02° in diffraction peak position determination was assumed, *i.e.* $\delta(2\theta) = 0.02°$.

As shown in Fig. 5(*a*), the best fit corresponds to the deformation E_{11}^{rol} = 7.5% when the χ^2 parameter reaches the minimum value. The poor agreement between the theoretical and the experimental data for $E_{11}^{rol} < 7.5\%$ can be explained by the gradual evolution of the incompatibility stresses, which increase from a zero value to higher values characteristic of stable elasto-plastic deformation. When the deformation is stable, *i.e.* starting from E_{11}^{rol} = 7.5%, the theoretical mean von Mises plastic incompatibility stress [$\sigma_{eq}^{g(ic)}$] [see equation (9)] becomes a linear function of the macrostrain E_{11}^{rol} (Fig. 5*b*). For deformations larger than E_{11}^{rol} = 7.5% the poor fit of the $\sin^2\psi$ plot (see Fig. 5*a*) is due to a significant modification of the crystallographic texture during calculations. In other words, the texture computed by the model differs significantly from the experimentally determined texture. Finally, the theoretical stresses calculated for E_{11}^{rol} = 7.5% were used in further analyses of the experimental data. It was verified that for this sample deformation the crystallographic texture does not change significantly (compare Figs. 4*a* and 4*b*).

3.3. Stresses determined during '*in situ*' tensile testing

Using the theoretical stresses $\overline{\sigma_{ij}^{g(ic)}}(\mathbf{g})$ calculated for macrostrain

E_{11}^{rol} = 7.5%, the fitting procedure based on equation (7) was applied to the data from the ULC96_1 and ULC96_2 samples (in as-received and loaded conditions, respectively), and the unknown adjusting parameters (*i.e.* σ_{ij}^{M}, q and d^0) were determined. An uncertainty of $\delta(2\theta) = 0.02^\circ$ was assumed in diffraction peak position determination. The earlier analysis of the plastic incompatibility stresses in a cold rolled ULC ferritic steel sample was only partially carried out by Baczmański *et al.* (1994), since the methodology was not sufficiently well developed at that time. Furthermore, the data from the '*in situ*' loaded sample could not be evaluated. Self-consistent calculations for a large number of grains (10^6) were not possible then, and consequently the incompatibility stresses and stored elastic energy were not determined for each orientation of polycrystalline grains in the case of a strongly textured material. The present work included the above aspects.

The results of the current analyses on ULC cold rolled samples in as-received (not loaded) condition are given in Table 3. Different types of diffraction elastic constants have been used in the analyses of the experimental data. In Figs. 6 and 7 the measured and the theoretical fitted curves for as-received (*a*) and for loaded samples (*b* and *c*) are shown. In the case of the loaded samples different tensile uniaxial stresses Σ_{11}^{ten}, within the elastic range of deformation, were applied to the ULC96_1 and ULC96_2 samples. The theoretical plots are obtained using two different assumptions, *viz*. (i) the plastic incompatibility stresses are not present (dashed lines, $q = 0$), and (ii) the influence of $\sigma_{ij}^{g(ic)}(\mathbf{g})$ stresses is taken into account and the q parameter is determined from equation (7) (continuous lines, $q \neq 0$). As seen in Figs. 6 and 7, the calculated lines definitely fit better to the experimental points when non-zero plastic incompatibility stresses are taken into account in the data analyses. The same conclusion can be drawn from Fig. 8, where the χ^2 parameter characterizing the quality of fitting is shown.

By analysing the obtained results, it was found that the nonlinearities of the $sin^2\psi$ plot are complex and depend on the sample elastic anisotropy (texture) and plastic incompatibility stresses. It should be noted that anisotropy of diffraction elastic constants alone did not account for the nonlinearities of the $sin^2\psi$ plots (see disagreement of the experimental points and dashed lines, especially in Fig. 6).

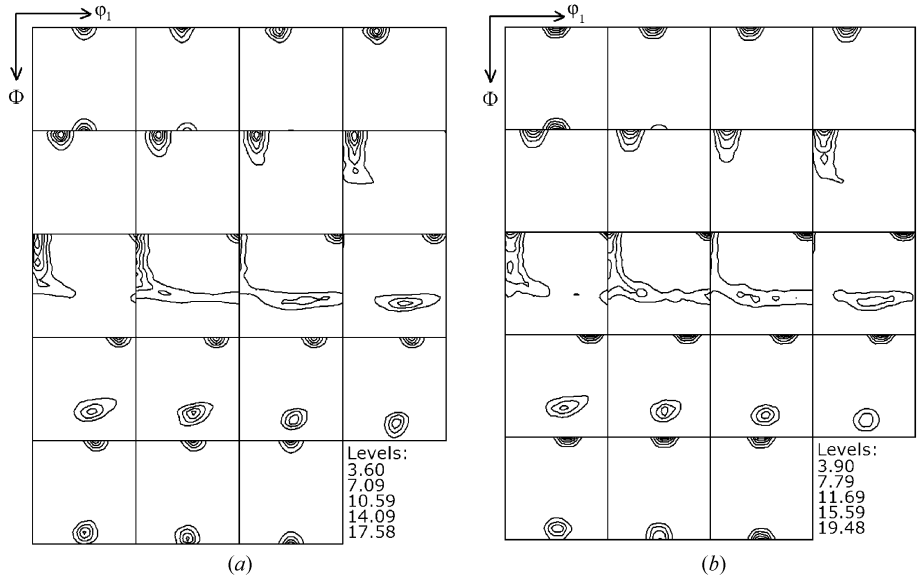

Figure 4
(*a*) Experimental orientation distribution function used as input data for the self-consistent model and (*b*) the predicted texture obtained after additional deformation E_{11}^{rol} = 7.5% of the cold rolling process. Sections through Euler space at intervals of 5° along the φ_2 axis are presented.

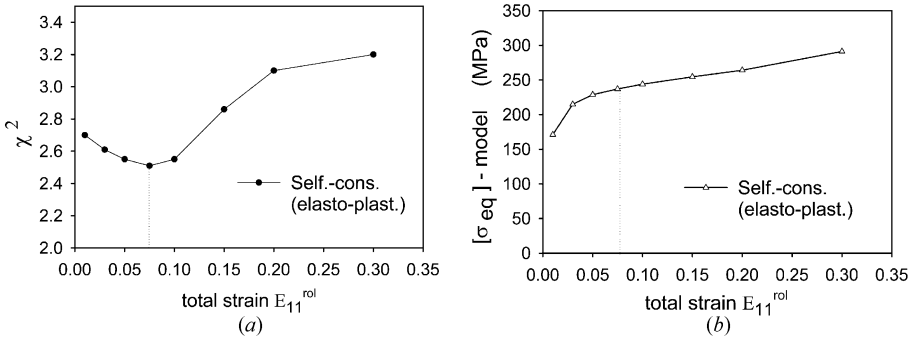

Figure 5
(*a*) Values of χ^2 characterizing the quality of fitting obtained when the model calculations were performed for different sample macrostrains E_{11}^{rol} of the cold rolling process, and (*b*) average equivalent von Mises plastic incompatibility stress $[\sigma_{eq}^{g(ic)}]$ *versus* total macrostrain E_{11}^{rol}, calculated by the self-consistent model.

3.4. Stress analysis using different types of diffraction elastic constants

The quality of fitting as characterized by the χ^2 parameter will depend on the type of diffraction elastic constants F_{ij} used in equation (7). The best agreement between the experimental and the theoretical results was found when the F_{ij} constants were calculated by the Reuss and the self-consistent free-surface models (Fig. 9). This confirms that the influence of sample elastic anisotropy on the nonlinearities of the $\langle d(\varphi, \psi)\rangle_{\{211\}}$ *versus* $\sin^2\psi$ curves is best predicted by these two approaches.

For a known q factor, the average equivalent von Mises stresses $[\sigma_{eq}^{g(ic)}]$ were estimated using equations (5) and (9). As shown in Fig. 10, the most stable (*i.e.* independent of the applied load) values of the equivalent plastic incompatibility stresses $[\sigma_{eq}^{g(ic)}]$ were obtained when the Reuss and the self-consistent

free-surface models were used to calculate the F_{ij} constants. When F_{ij} constants calculated by other models (*i.e.* the Voigt and the self-consistent approach for a sample interior) are used in the fitting procedure, the determined value of $[\sigma_{eq}^{g(ic)}]$ stress strongly depends on the value of the external stress applied to the sample. In such cases, the anisotropy of the diffraction elastic constants is not correctly predicted and the nonlinearities of the $\langle d(\varphi, \psi)\rangle_{\{211\}}$ *versus* $\sin^2\psi$ curves are interpreted mostly as the effect of plastic incompatibilities. Consequently, the values of $[\sigma_{eq}^{g(ic)}]$ are artificially increased or decreased and they significantly depend on the applied stress Σ_{11}^{ten} (Fig. 10).

For every sample there exists a value of the applied load (Σ_{11}) at which the determined $[\sigma_{eq}^{g(ic)}]$ stress does not depend on the type of the diffraction elastic constants used (intersection point of all lines in Fig. 10). This applied stress Σ_{11}^{ten} compensates the component σ_{11}^{M} of residual macrostress acting in the as-received samples. When $\Sigma_{11}^{ten} \simeq -\sigma_{11}^{M}$, the influence of

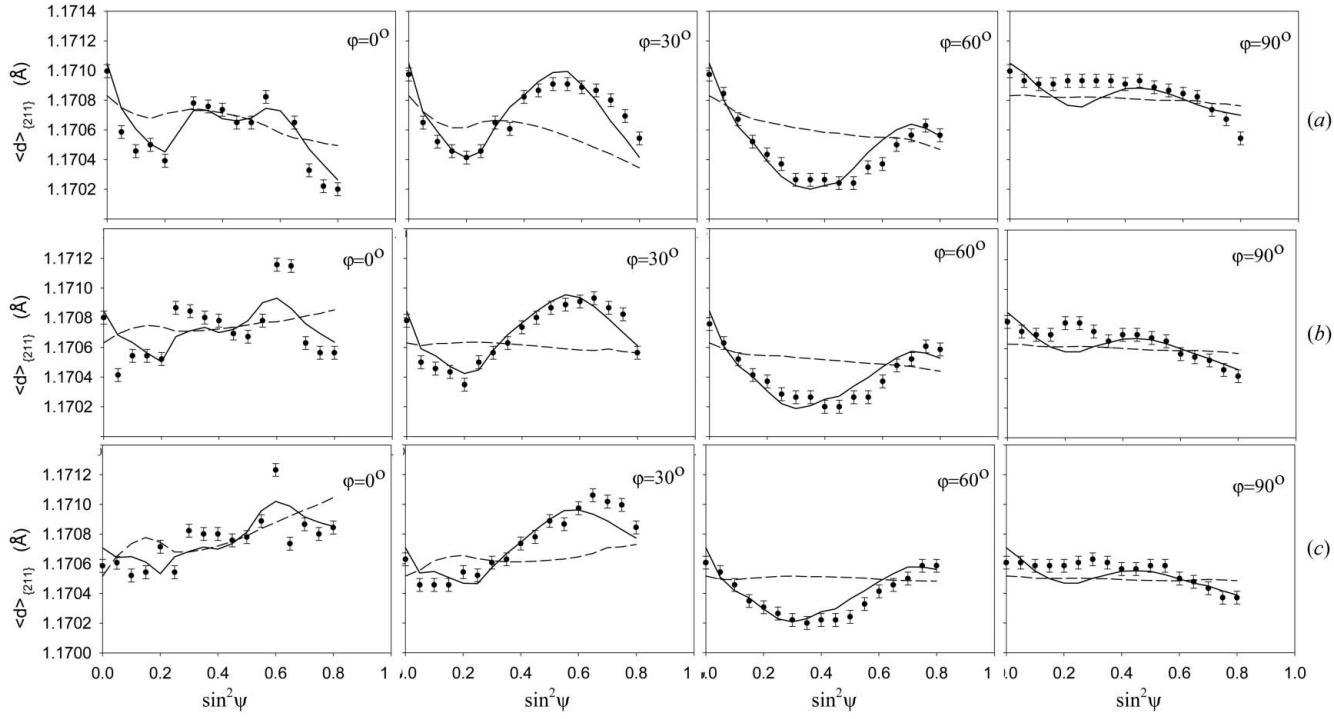

Figure 6
Measured lattice parameters (points) and theoretical results of fitting (continuous lines for $q \neq 0$ and dashed lines for $q = 0$) for the ULC96_1 sample (see Table 3). The results are presented for (*a*) the as-received sample, (*b*) superimposed tensile stress Σ_{11}^{ten} = 90 MPa and (*c*) Σ_{11}^{ten} = 150 MPa. The self-consistent free-surface method was used for calculation of the diffraction elastic constants. The error bars correspond to $\delta(2\theta) = 0.02^\circ$.

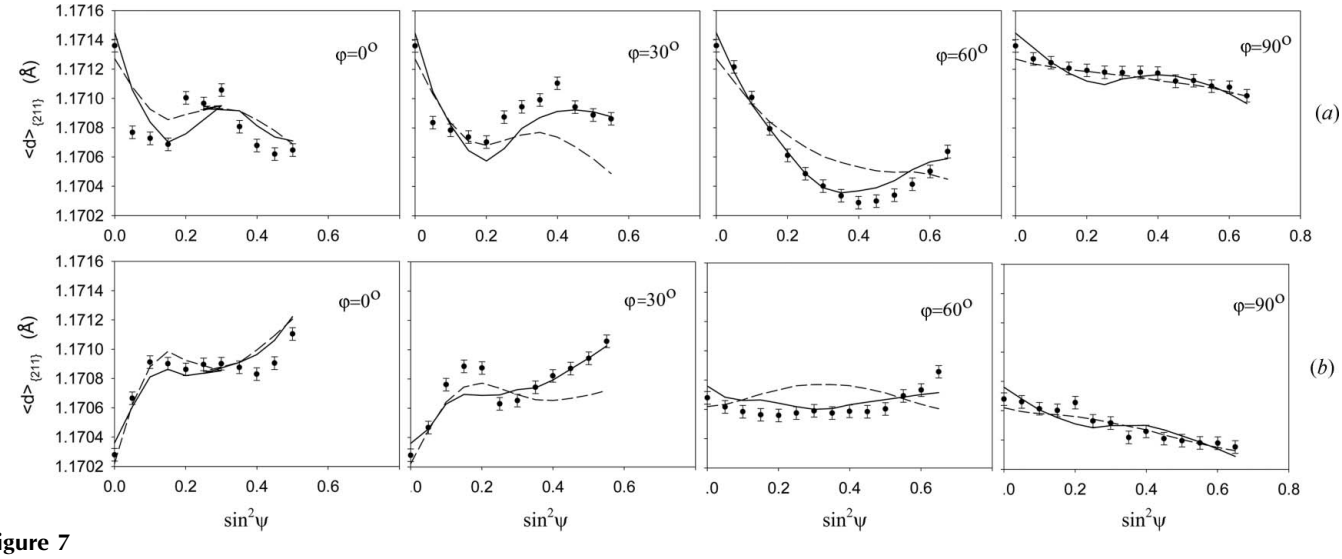

Figure 7
Measured lattice parameters (points) and theoretical results of fitting (continuous lines for $q \neq 0$ and dashed lines for $q = 0$) for the ULC96_2 sample (see Table 3). The results are presented for (*a*) the as-received sample and (*b*) superimposed tensile stress Σ_{11}^{ten} = 400 MPa. The self-consistent free-surface method was used for calculation of the diffraction elastic constants. The error bars correspond to $\delta(2\theta) = 0.02^\circ$.

Table 3
Results of fitting procedure for ULC96 as-received samples [errors correspond to uncertainty in peak position, $\delta(2\theta) = 0.02^\circ$].

Calculations were performed taking into account plastic incompatibility stresses. The values of the χ^2 parameter obtained neglecting plastic incompatibility stresses are given in {} brackets. $[\sigma_{eq}^{IIg(ic)}]$ is the average equivalent plastic incompatibility stress and $d_{\{211\}}^0$ is the stress-free interplanar spacing.

Sample	Type of diffraction elastic constants used	Macrostresses (MPa) σ_{11}^M	σ_{22}^M	σ_{12}^M	q	$[\sigma_{eq}^{IIg(ic)}]$ (MPa)	$d_{\{211\}}^0$ (Å)	$\chi^2(q \neq 0)$ $\{\chi^2(q = 0)\}$
ULC96_1 (200 µm removed)	Reuss	−53 (9)	−39 (10)	−4 (8)	0.54 (3)	128 (4)	1.17061 (4)	2.5 {12.1}
	Self-consistent (free surface)	−53 (10)	−39 (10)	−4 (9)	0.54 (3)	127 (4)	1.17061 (4)	2.6 {12.2}
	Self-consistent (interior)	−49 (10)	−35 (10)	−9 (9)	0.57 (3)	134 (4)	1.17061 (4)	2.6 {14.3}
	Voigt	−43 (10)	−33 (10)	−12 (9)	0.58 (3)	138 (4)	1.17062 (4)	2.8 {15.5}
ULC96_2 (100 µm removed)	Reuss	−183 (24)	−88 (19)	−26 (17)	0.52 (7)	111 (15)	1.17063 (8)	3.0 {7.6}
	Self-consistent (free surface)	−182 (25)	−80 (19)	−34 (17)	0.51 (7)	109 (14)	1.17063 (8)	3.1 {7.5}
	Self-consistent (interior)	−150 (25)	−65 (18)	−39 (17)	0.67 (7)	143 (13)	1.17067 (8)	3.5 {12.7}
	Voigt	−120 (25)	−51 (19)	−48 (17)	0.76 (7)	162 (14)	1.17070 (8)	4.1 {16.4}

the diffraction elastic constants on the $\langle d(\varphi, \psi)\rangle_{\{211\}}$ *versus* $\sin^2\psi$ curves and on the determined $[\sigma_{eq}^{g(ic)}]$ stresses is minimized. This is due to the small net resultant macrostress after superposition of the applied and the residual stresses. The residual stresses σ_{11}^M in the as-received samples, deduced from intersection points in Fig. 10 (*i.e.* about 200 MPa for the ULC96_1 and 45 MPa for the ULC96_2 samples) are approximately equal to those determined by the modified $\sin^2\psi$ method with Reuss and self-consistent free-surface diffraction elastic constants (*i.e.* about 182 MPa for the ULC96_1 and 53 MPa for the ULC96_2 samples; see Table 3). Such agreement proves that the macrostresses in plastically deformed samples can be accurately determined using the modified $\sin^2\psi$ method (accounting for the presence of plastic incompatibility stresses and crystallographic texture).

In Fig. 11 the values of the stress-free interplanar spacing $d_{\{211\}}^0$ versus applied loads are presented for both studied samples. It is important to note that the value of $d_{\{211\}}^0$ does not depend significantly on the values of the stresses present in the sample (the $d_{\{211\}}$ range is kept the same in Figs. 6, 7 and 11 for an easy comparison). Thus the proposed method offers an additional advantage of determining the stress-free lattice parameter for samples containing significant macrostresses and plastic incompatibility stresses.

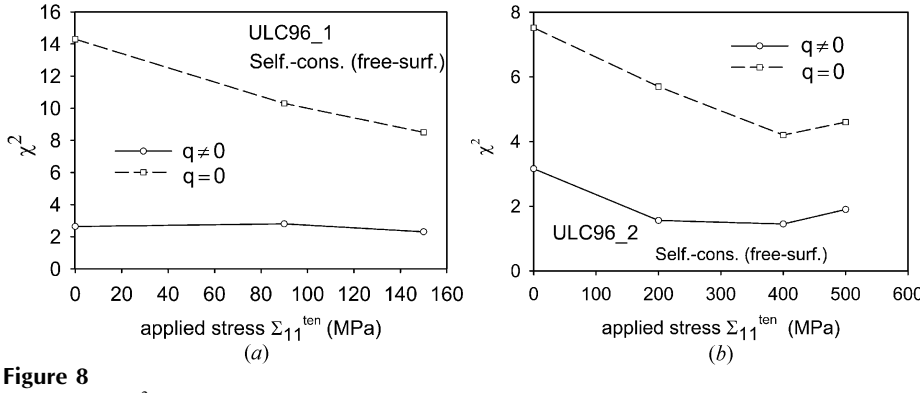

Figure 8
Values of the χ^2 parameter obtained when the plastic incompatibility stresses were neglected ($q = 0$) or were taken into account ($q \neq 0$) in the fitting procedure based on equation (7). The results for as-received and '*in situ*' loaded (*a*) ULC96_1 and (*b*) ULC96_2 samples are shown.

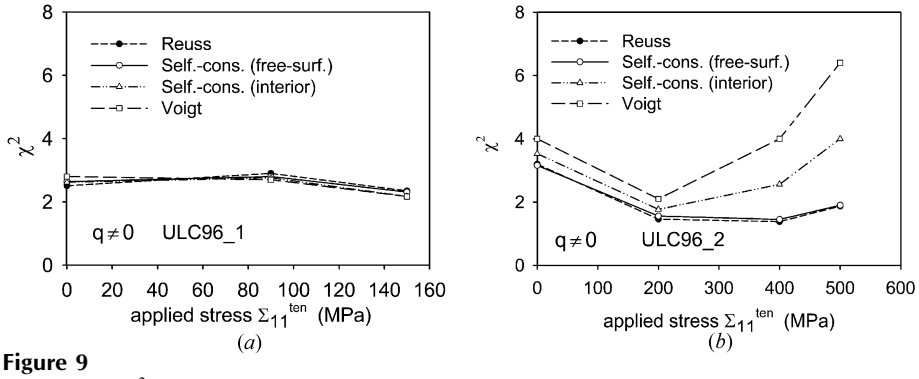

Figure 9
Values of the χ^2 parameter obtained when different types of diffraction elastic constants were used in the fitting procedure based on equation (7). The results for as-received and '*in situ*' loaded (*a*) ULC96_1 and (*b*) ULC96_2 samples are shown.

Finally, the possibility of determining the macrostress tensor was evaluated using the data obtained at different applied loads. In fact, it is impossible to verify the absolute values of the residual macrostresses present in the samples in the as-received condition. However, the differences between the determined macrostresses can be compared with the corresponding applied stresses. In Fig. 12 the re-evaluated stresses Σ_{ij}^E as a function of the applied stress Σ_{11}^{ten} is presented. The re-evaluated stress is defined as

$$\Sigma_{ij}^E = \sigma_{ij}^M(\Sigma_{11}^{ten}) - \sigma_{ij}^M(0), \qquad (18)$$

where $\sigma_{ij}^M(0)$ and $\sigma_{ij}^M(\Sigma_{11}^{ten})$ are the macrostresses determined in the as-received and in the Σ_{11}^{ten} stress-applied conditions, respectively.

It was verified (Fig. 12) that the values of the applied stresses were

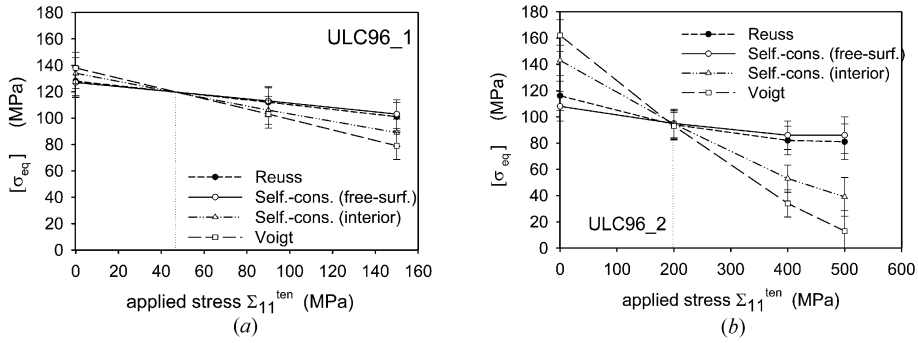

Figure 10
Values of average equivalent stress $[\sigma_{eq}^{g(ic)}]$ obtained when different types of the diffraction elastic constants were used in the fitting procedure based on equation (7). The results for as-received and '*in situ*' loaded (*a*) ULC96_1 and (*b*) ULC96_2 samples are shown.

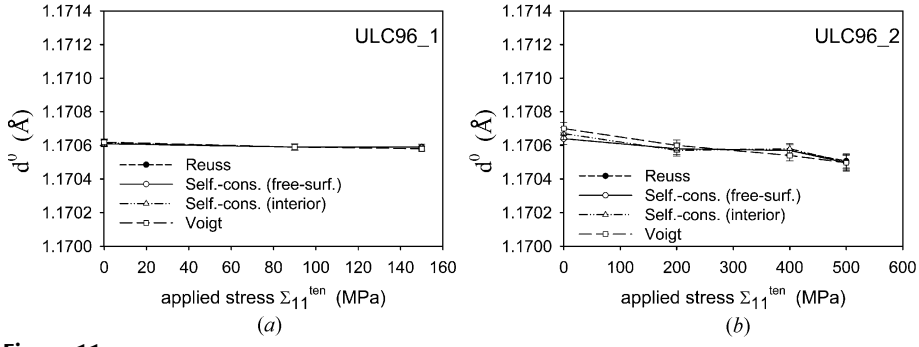

Figure 11
Values of the stress-free interplanar spacing $d_{\{211\}}^{0}$ obtained when different types of diffraction elastic constants were used in the fitting procedure based on equation (7). The results for as-received and '*in situ*' loaded (*a*) ULC96_1 and (*b*) ULC96_2 samples are shown.

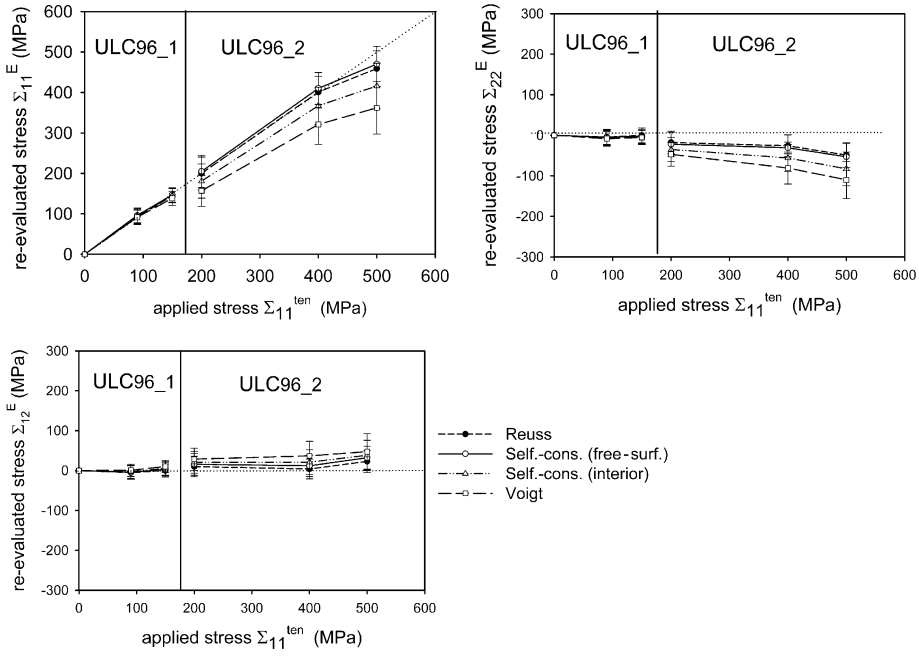

Figure 12
Values of re-evaluated stresses Σ_{ij}^{E} determined using different types of the diffraction elastic constants.

precisely re-evaluated when the Reuss model or the self-consistent model for a free surface were used to calculate the diffraction elastic constants. The values of the applied stresses were correctly re-evaluated (below Σ_{11}^{ten} = 400 MPa), *i.e.*

$$\Sigma_{11}^{E} \simeq \Sigma_{11}^{ten},\ \Sigma_{22}^{E} \simeq 0 \text{ and } \Sigma_{12}^{E} \simeq 0. \tag{19}$$

Only for Σ_{11}^{ten} = 500 MPa is the re-evaluated stress smaller than the applied one (Fig. 12), probably as a result of local plasticity occurring when the superposed stresses exceed the elastic limit. Consequently, it can be concluded that the present method can be used to determine macrostresses in anisotropic (textured) samples and in the presence of plastic incompatibility stresses.

4. Stress and energy orientation distribution functions

By using the q factor obtained from the fitting procedure in equation (5), the values of the plastic incompatibility residual stresses for each orientation of a polycrystalline grain can be calculated. For complete results, six components of the stress tensor should be shown in Euler space. In the case of the cold rolled samples (bcc structure) analysed, it is sufficient to show the stresses using only one section of the Euler space ($0^\circ \leq \varphi_1 \leq 90^\circ$, $0^\circ \leq \Phi \leq 90^\circ$ and $\varphi_2 = 45^\circ$), since this section contains all main texture components.

The model calculations were performed for a large number of orientations (10^6 grains) in order to have good statistical information about the stress values at all points of a mesh created in Euler space with a step of 5° for the φ_1, Φ and φ_2 angles. The experimental texture (Fig. 3*a*) and the initial parameters shown in Table 2 were used in the calculations. A scaling factor of q = 0.54 was used (the same value as was used for 10 000 grains) in equation (7) to determine the plastic incompatibility stresses. In Fig. 13, the contour plots of the orientation distribution function $f(\mathbf{g})$, the equivalent von Mises stress $\sigma_{eq}^{g(ic)}(\mathbf{g})$ [as defined in

equation (9)] and the stored elastic energy are presented. The stored elastic energy was calculated using the formula

$$W^{g(ic)}(\mathbf{g}) = (1/2)\,\sigma_{ij}^{g(ic)}(\mathbf{g})\,s_{ijkl}^{g}(\mathbf{g})\,\sigma_{kl}^{g(ic)}(\mathbf{g}), \qquad (20)$$

where $s_{ijkl}^{g}(\mathbf{g})$ is the compliance tensor of a grain having the lattice orientation $\mathbf{g}$.

In Fig. 14 the components of the stress tensor $\sigma_{ij}^{g(ic)}(\mathbf{g})$ are shown. In Figs. 13 and 14, the areas with high density of orientations (texture) are indicated in grey.

As seen in Fig. 13(*c*), the elastic energy $W^{g(ic)}(\mathbf{g})$ is not equally distributed among different orientations. The highest energy is stored in the grains having lattice orientations close to the texture components $\{112\}\langle 1\bar{1}0\rangle$ (component *A* in Fig. 13), while the energy minimum corresponds to the group of symmetrical orientations $\{111\}\langle 1\bar{2}1\rangle$ (components *Y* and *Y** in Fig. 13). Other preferred orientations ($\{001\}\langle 1\bar{1}0\rangle$ and $\{111\}\langle 1\bar{1}0\rangle$, *i.e.* *R*, *R** and *Z*, *Z**, respectively) exhibit the average value of energy. As shown in Fig. 13(*b*), the dependence of the equivalent von Mises stress $\sigma_{eq}^{g(ic)}(\mathbf{g})$ on the lattice orientation is similar to that seen with the elastic energy $W^{g(ic)}(\mathbf{g})$.

Interesting conclusions can be drawn when the dependence of the stress components $\sigma_{ij}^{g(ic)}(\mathbf{g})$ on the lattice orientation is studied. By applying the Schmid law to cold rolled bcc materials, the resolved shear stresses for different slip systems were compared by Shiraiwa & Sakamoto (1970). They found that the crystals having $\{111\}\langle 1\bar{2}1\rangle$ and $\{001\}\langle 1\bar{1}0\rangle$ lattice orientations are the most difficult and the most easy to deform, respectively. This observation is now confirmed by this study when applying the self-consistent model. In the results presented in Fig. 14, the negative value of the component $\sigma_{11}^{g(ic)}(\mathbf{g})$ indicates the lattice orientations of the grains that are more plastically elongated along the rolling direction (in comparison with the average sample deformation in this direction). These grains have lattice orientations around $\{001\}\langle 1\bar{1}0\rangle$ (*i.e.* *R* and *R** in Fig. 14) and correspond to orientations for which the maximum resolved shear stress for active slip exhibits the largest value. Thus, the plastic deformation in grains with orientations close to $\{001\}\langle 1\bar{1}0\rangle$ occurs easily, which produces incompatibility back stress (compressive) having the opposite sign with respect to the macrostress applied along the rolling direction (tensile). Conversely, for $\{111\}\langle 1\bar{1}0\rangle$ and $\{111\}\langle 1\bar{2}1\rangle$ (*Z*, *Z** and *Y*, *Y**) lattice orientations the maximum value of the resolved shear stress is relatively low. Hence these grains are less deformed along the rolling direction than the average volume of the sample and tensile incompatibility stresses are created in this direction. For lattice orientations that are close to the $\{112\}\langle 1\bar{1}0\rangle$ (*i.e.* *A* in Fig. 14) texture component, the smallest value of the $\sigma_{11}^{g(ic)}(\mathbf{g})$ residual stress has been found. This means that the elasto-plastic deformations of grains having that lattice orientation are approximately equal to the macrostrain of the whole sample (consequently the grain incompatibilities are small).

When comparing the $\sigma_{33}^{g(ic)}(\mathbf{g})$ and $\sigma_{11}^{g(ic)}(\mathbf{g})$ incompatibility

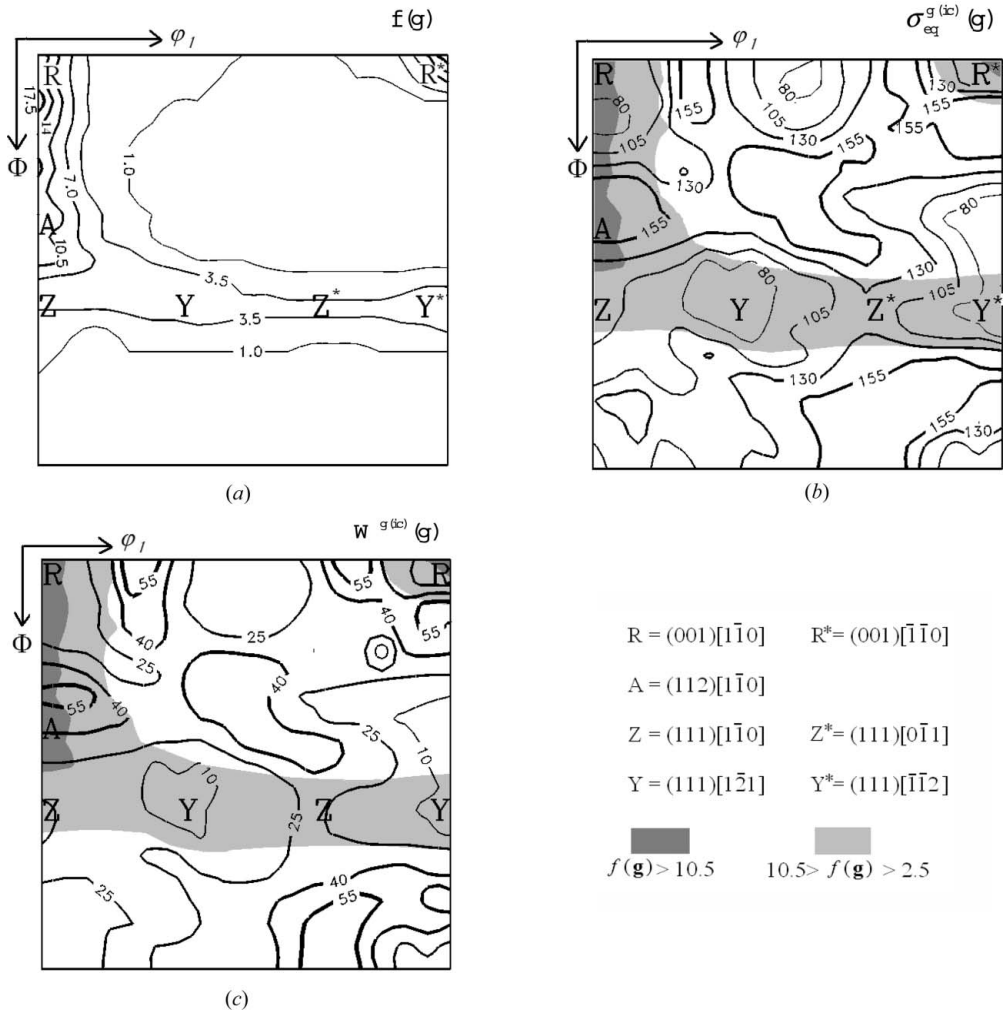

Figure 13
Contour plots of (*a*) the orientation distribution function $f(\mathbf{g})$, (*b*) the equivalent von Mises stress $\sigma_{eq}^{g(ic)}(\mathbf{g})$ (MPa) and (*c*) the stored elastic energy $W^{g(ic)}(\mathbf{g})$ (kJ m^{-3}) presented in the section $\varphi_2 = 45°$. The following notation is used for the main texture components: (*hkl*) is the crystallographic plane parallel to the surface of the sheet and [*uvw*] is the crystallographic direction parallel to the rolling direction (RD). The grey shaded areas in plots (*b*) and (*c*) indicate a high density of orientations.

stresses, the opposite signs of these components have been found for the same lattice orientation **g**. During the rolling process, the macrostresses applied to the sample in the normal and the rolling directions have opposite signs (compression in the normal direction and tension in the rolling direction). The tensile stress $\sigma_{33}^{g(ic)}(\mathbf{g})$ confirms that the plastic deformation occurs more easily for the $\{001\}\langle 1\bar{1}0\rangle$ than for the $\{111\}\langle 1\bar{1}0\rangle$ and $\{111\}\langle 1\bar{2}1\rangle$ lattice orientations for which the compressive values of the $\sigma_{33}^{g(ic)}(\mathbf{g})$ stress are observed. Almost zero $\sigma_{33}^{g(ic)}(\mathbf{g})$ stress was found for the grains having the $\{112\}\langle 1\bar{1}0\rangle$ lattice orientation, confirming small plastic incompatibilities for those grains.

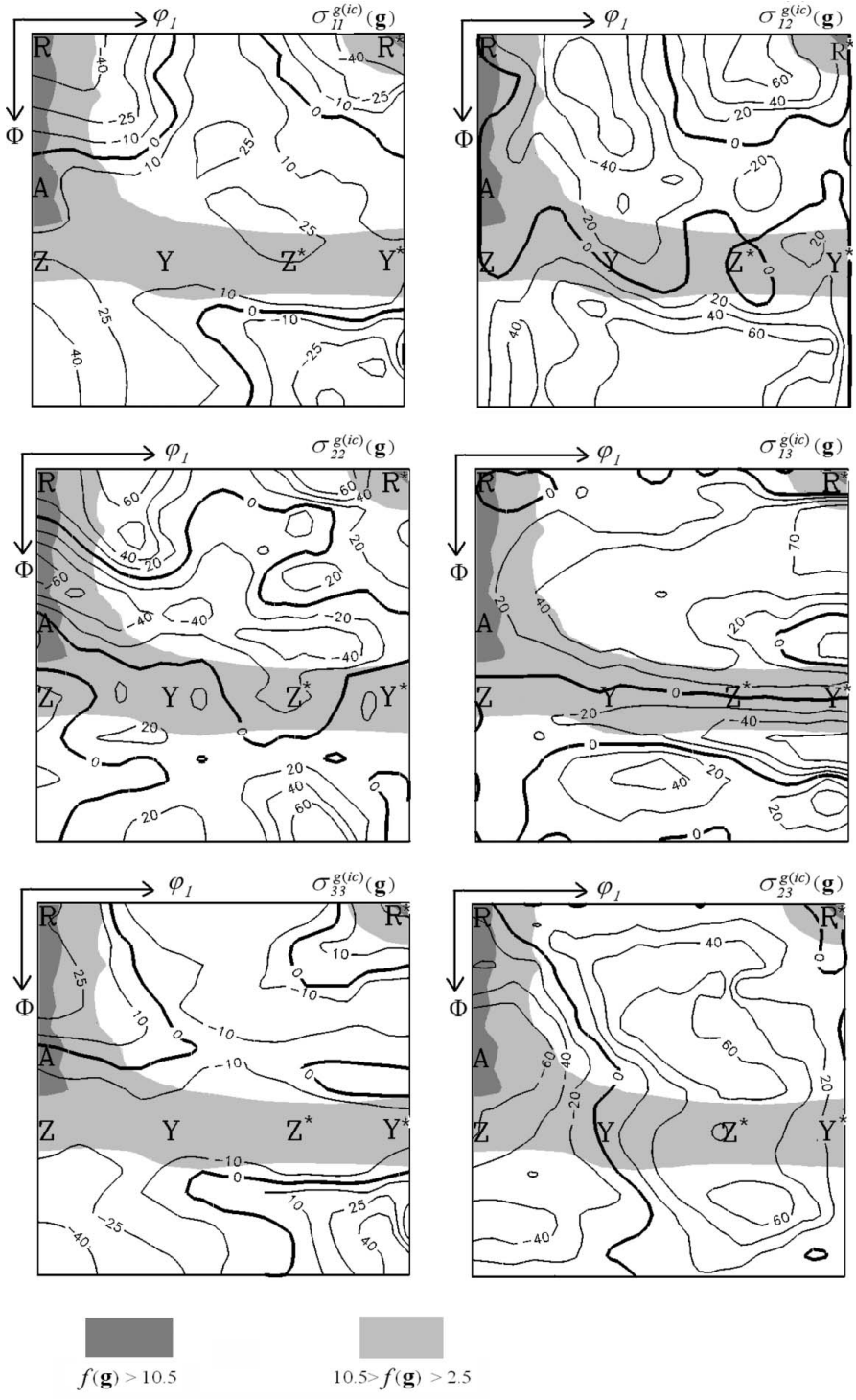

Figure 14
Components of the stress tensor $\sigma_{ij}^{g(ic)}(\mathbf{g})$ (MPa) presented in the section $\varphi_2 = 45^\circ$. The main texture components and the areas of high density of orientations (grey shaded areas) are indicated.

When analysing the shear components of plastic incompatibility stresses, near zero values of $\sigma_{13}^{g(ic)}(\mathbf{g})$ and $\sigma_{12}^{g(ic)}(\mathbf{g})$ stresses were found for all main texture components. In contrast, significant absolute values of the $\sigma_{23}^{g(ic)}(\mathbf{g})$ stress component were determined for the $\{111\}\langle 1\bar{1}0\rangle$ and $\{112\}\langle 1\bar{1}0\rangle$ orientations (Z, Z^* and A components in Fig. 14), and near zero values of the $\sigma_{23}^{g(ic)}(\mathbf{g})$ stress for the $\{111\}\langle 1\bar{2}1\rangle$ and $\{001\}\langle 1\bar{1}0\rangle$ orientations (Y, Y^*, R and R^* components in Fig. 14). It should be mentioned that the $\sigma_{23}^{g(ic)}(\mathbf{g})$ stresses for the Z and Z^* orientations have opposite signs because of the sample symmetries imposed on the stress tensor [the symmetries for the stress tensor are different from those defined for the scalar orientation distribution function $f(\mathbf{g})$; see Wang *et al.* (1999)]. The shear components of the determined stress tensor show that the x principal axis of the incompatibility stresses is parallel to the rolling direction for all main texture components. For orientations $\{111\}\langle 1\bar{2}1\rangle$ (*i.e.* Y) and $\{001\}\langle 1\bar{1}0\rangle$ (R), the y and z principal axes coincide with the transverse and normal directions, respectively. However, in the case of the $\{111\}\langle 1\bar{1}0\rangle$ (Z) and $\{112\}\langle 1\bar{1}0\rangle$ (A) orientations, the y and z principal axes of the stresses are significantly tilted from the transverse and normal directions [significant values of the shear stresses $\sigma_{23}^{g(ic)}(\mathbf{g})$ were determined].

It should be emphasized that the above-described variations in incompatibility stress are caused by the anisotropy in plastic and elastic deformations of grains and cannot be easily interpreted without the self-consistent model.

The values of incompatibility stresses determined in the present work were quantitatively compared with those measured by the neutron diffraction method for a similar sample (Pintschovius *et al.*, 1987). To measure the plastic incompatibility stresses, Pintschovius *et al.* (1987) determined lattice strains for various *hkl* reflections and for particular directions of the scattering vector corre-

sponding to the main texture components. The mean stresses over the whole cross section of the sheet were determined using a large gauge volume. This method enabled the authors to find the stress tensor only for particular orientations of a strongly textured sample. Similar conclusions concerning shear stresses and orientations of principal stress axes were drawn for all considered texture orientations. In addition, a very good agreement between the neutron results and the present data was found for the $\sigma_{22}^{g(ic)}(\mathbf{g})$ stress for different texture components. In the case of the $\sigma_{11}^{g(ic)}(\mathbf{g})$ and $\sigma_{33}^{g(ic)}(\mathbf{g})$ stress components, a direct comparison cannot be made since, in the case of neutron diffraction measurements, non-zero macrostresses in the rolling and transverse directions were found and the plastic incompatibility stresses were not determined.

5. General conclusions

In the present study, the modified $\sin^2\psi$ diffraction method (Baczmański *et al.*, 1994) for determination of the stresses in polycrystalline material was further developed. In the current version of the method, the theoretical plastic incompatibility stresses are calculated by the self-consistent model starting from the experimental texture data. It has been shown that, after a relatively small plastic deformation (7.5%), the non-linearities in $\langle d(\varphi, \psi)\rangle_{\{211\}}$ *versus* $\sin^2\psi$ curves are correctly predicted. The best fitting of the model predictions with experimental results is obtained by minimizing the value of the merit function χ^2. The advantage of this new methodology is that the calculations can be performed for grain orientations determined from experimental texture and consequently the sample anisotropy is correctly defined.

The methodology was also enriched by incorporating a new type of X-ray diffraction elastic constant. Using a new approach, the relaxation of the stresses perpendicular to the sample surface is considered and the free-surface self-consistent model is introduced. Previously, the new diffraction elastic constants were successfully tested for cold rolled steel (Baczmański *et al.*, 2006).

For the first time, the modified $\sin^2\psi$ method was tested on samples subjected to known external tensile loads. It has been demonstrated that, by using this method, such applied macrostresses can be accurately re-evaluated and separated from the plastic incompatibility stresses for strongly textured samples. It has been shown that the values of the applied macrostresses are precisely re-evaluated when the Reuss or the self-consistent method for a free surface are used to calculate the diffraction elastic constants. The latter results also showed that reasonable values of the diffraction constants can be obtained when the directional dependence of the grains' interaction is considered in the self-consistent model.

The tests performed with the modified $\sin^2\psi$ method allowed us to select an optimal plastic sample strain $E_{11}^{rol} = 7.5\%$ for model prediction and to chose the free-surface self-consistent diffraction elastic constants for an analysis of the residual stresses in as-received ULC ferritic steel samples. The tensor of plastic incompatibility stress $\sigma_{ij}^{g(ic)}(\mathbf{g})$ has been found for each orientation of a polycrystalline grain and the results are presented in Euler space. In this simulation, a great number (10^6) of grains were used. The obtained grain stresses agree with the results from previous work where the stresses were determined for different groups of grain orientations. Finally, for the first time the distribution of elastic energy $W^{g(ic)}(\mathbf{g})$ (caused by plastic incompatibilities between grains) was determined for cold rolled ferritic steel, and the results are shown in Euler space.

In conclusion, it should be emphasized that the advantage of the modified $\sin^2\psi$ method is that *quantitative values* of incompatibility stresses and stored elastic energy can be determined for *all orientations* of the crystallite lattice without any assumptions. The previous methods provided only qualitative indications. They gave no unique solution and enabled measurement of stresses only for a few particular orientations of strongly textured samples.

This research project was supported by the Polish Ministry of Science and Higher Education (MNiSW) and by the European Union through the European Network of Excellence 'Complex Metallic Alloys' (EU 6th Framework Programme).

References

Baczmański, A., Braham, C. & Seiler, W. (2003). *Philos. Mag.* **83**, 3225–3246.
Baczmański, A., Braham, C. & Seiler, W. (2004). *Phys. Status Solidi A*, **201**, 2886–2899.
Baczmański, A., Skrzypek, S. J., Braham, C., Seiler, W. & Wierzbanowski, K. (2003). *Arch. Metall.* **48**, 137–149.
Baczmański, A., Tidu, A., Lipinski, P., Humbert, M. & Wierzbanowski, K. (2006). *Mater. Sci. Forum*, **524–525**, 235–240.
Baczmański, A., Wierzbanowski, K., Haije, W. G., Helmholdt, R. B., Ekambaranathan, G. & Pathiraj, B. (1993). *Cryst. Res. Technol.* **28**, 229–246.
Baczmański, A., Wierzbanowski, K., Lipinski, P., Helmholdt, R. B., Ekambaranathan, G. & Pathiraj, B. (1994). *Philos. Mag. A*, **69**, 437–443.
Baczmański, A., Wierzbanowski, K., Tarasiuk, J., Ceretti, M. & Lodini, A. (1997). *Rev. Metall.* **42**, 1467–1474.
Barral, M., Lebrun, J. L., Sprauel, J. M. & Maeder, G. (1987). *Met. Trans. A*, **18**, 1229–1238.
Behnken, H. (2000). *Phys. Status Solidi A*, **177**, 401–418.
Behnken, H. (2002). *Mater. Sci. Forum*, **404–407**, 275–280.
Brakman, C. M. (1987). *Philos. Mag. A*, **55**, 39–58.
Bunge, H. J. (1982). *Texture Analysis in Materials Science: Mathematical Methods.* London: Butterworths.
Clyne, T. W. & Withers, P. J. (1993). *An Introduction to Metal Matrix Composites*, Cambridge Solid State Science Series. Cambridge University Press.
Dölle, H. (1979). *J. Appl. Cryst.* **12**, 489–501.
Greenough, G. B. (1949). *Proc. R. Soc. London Ser. A*, **197**, 556–567.
Hauk, V. (1986). *Adv. X-ray Anal.* **29**, 1–15.
Hauk, V. (1997). *Structural and Residual Stress Analysis by Nondestructive Methods*. Amsterdam: Elsevier.
Hauk, V., Krug, W. K., Oudelhoven, W. M. & Pintschovius, L. (1988). *Z. Metallkd.* **79**, 159–167.
Inal, K., Gergaud, P., Francois, M. & Lebrun, J.-L. (1999). *Scand. J. Metall.* **28**, 139–150.
Kneer, G. (1965). *Phys. Status Solidi*, **9**, 825–838.

Krier, J. (1993). PhD thesis, Universite de Metz, France.
Kröner, E. (1961). *Acta Metall.* **9**, 155–161.
Lipinski, P. & Berveiller, M. (1989). *Int. J. Plast.* **5**, 149–172.
Marion, R. H. & Cohen, J. B. (1977). *Adv. X-ray Anal.* **20**, 355–367.
Matthies, S. & Humbert, M. (1995). *J. Appl. Cryst.* **28**, 254–266.
Mura, T. (1993). *Micromechanics of Defects in Solids*. Dordrecht, Boston, London: Kluwer Academic Publishers.
Noyan, I. C. & Cohen, J. B. (1987). *Residual Stress – Measurement by Diffraction and Interpretation*. Berlin: Springer-Verlag.
Pintschovius, L., Hauk, V. & Krug, W. K. (1987). *Mater. Sci. Eng.* **92**, 1–12.
Reuss, A. (1929). *Z. Angew. Math. Mech.* **9**, 49–58.
Shiraiwa, T. & Sakamoto, Y. (1970). Proceedings of the 13th Japanese Congress on Materials Research – Metallic Materials, Kyoto, Japan, pp. 25–32.
Taira, S., Hayashi, K. & Urakawa, N. (1971). *J. Jpn Inst. Met.* **35**, 189–196.
Van Acker, K., Van Houtte, P. & Aernoudt, E. (1994). Proceedings of the 4th International Conference on Residual Stresses, ICRS4, Society for Experimental Mechanics Inc., Baltimore, Maryland, USA, pp. 402–409.
Van Leeuwen, M., Kamminga, J.-D. & Mittemeijer, E. J. (1999). *J. Appl. Phys.* **86**, 1904–1914.
Voigt, W. (1928). *Lehrbuch der Kristallphysik*. Leipzig: BG Teubner, Verlag.
Wang, Y. D., Lin Peng, R. & McGreevy, R. (1999). *Scr. Mater.* **41**, 995–1000.
Wang, Y. D., Lin Peng, R. & McGreevy, R. (2001). *Philos. Mag. Lett.* **81**, 153–163.
Wang, Y. D., Wang, X.-L., Stoica, A. D., Richardson, J. W. & Lin Peng, R. (2003). *J. Appl. Cryst.* **36**, 14–22.
Welzel, U. & Fréour, S. (2007). *Philos. Mag.* **87**, 3921–3943.
Welzel, U., Leoni, M. & Mittemeijer, E. J. (2003). *Philos. Mag.* **83**, 603–630.
Welzel, U., Ligot, J., Lamparter, P., Vermeulen, A. C. & Mittemeijer, E. J. (2005). *J. Appl. Cryst.* **38**, 1–29.
Willemse, P. F., Naughton, B. P. & Verbraak, C. A. (1982). *Mater. Sci. Eng.* **56**, 25–37.
Witt, F. & Vook, R. W. (1968). *J. Appl. Phys.* **39**, 2773–2776.
Wroński, S., Baczmański, A., Dakhlaoui, R., Braham, C., Wierzbanowski, K. & Oliver, E. C. (2007). *Acta Mater.* **55**, 6219–6233.
Zattarin, P., Baczmański, A., Lipiński, P. & Wierzbanowski, K. (2000). *Arch. Metall.* **45**, 163–184.